SUPPLEMENTARY MATERIAL

TITLE: Arrhythmogenic Remodelling of the Right Ventricle in a Porcine Model of Repaired Tetralogy of Fallot

Authors: David Benoist, PhD; Virginie Dubes, MSc; François Roubertie, MD, PhD; Stephen H. Gilbert, PhD; Sabine Charron, MSc; Marion Constantin, MSc; Delphine Elbes, PhD; Delphine Vieillot, TA; Bruno Quesson, PhD; Hubert Cochet, MD, PhD; Michel Haïssaguerre, MD; Caroline Rooryck, MD, PhD; Pierre Bordachar, MD, PhD; Jean-Benoit Thambo, MD, PhD; Olivier Bernus, PhD

SUPPLEMENTARY METHODS

Animal Model

The animal model of repaired TOF (rTOF N=6) was produced as previously described.[1] Briefly, Large White piglets (< 12kg) were pre-medicated with ketamine (10 mg/kg, IM, Vibrac) and acepromazine (0.1 mg/kg, Vetoquinol). Anesthesia was induced with sodium pentobarbital (5 mg/kg, IV, Ceva) and maintained with isoflurane (2% in 100% O_2, Vibrac) after endotracheal intubation. The anterior side of the heart was accessed by lateral thoracotomy. The pulmonary artery was longitudinally clamped, a 2 cm incision was made across the pulmonary annulus and 2 pulmonary valve leaflets were excised. A PTFE patch was sewn across the annulus and pulmonary artery banding was performed using a loose-tied tape (2 cm diameter). For sham-operated animals, only the lateral thoracotomy was performed (Sham N=4). At the end of the procedure, piglets received supplemental oxygen and analgesia as appropriate before their transfer to the animal house. Cardiac function and remodelling was assessed 23 ± 1 weeks post-surgery as detailed below.

Cardiac Magnetic Resonance Imaging

Pigs were pre-medicated and anaesthetised as described above. A conventional cardiac magnetic resonance (CMR) examination was carried out as described in Bogaert et al,[2] using a Siemens Magnetom Avanto 1.5T MRI scanner (Erlangen, Germany) with maximum gradient strength of 200 mT/m and a slew rate of 45 mT/m/ms. Briefly, pigs were placed in dorsal recumbancy (supine) and ECG leads placed after shaving and hair removal with thioglycolic acid/KOH cream (Veet, Reckitt Benckiser, UK) and the telemetric vector electrocardiogram was used for gating of the Siemens CMR sequences. All images were taken during end-expiratory ventilation stop. Localiser views were followed by right-ventricular short-axis TrueFISP cine-image stacks (from the cardiac apex to the level of the pulmonary valve) under manual-breathhold. For pulmonary artery flow measurement phase-contrast MRI was carried out under manual-breathhold with the velocity encoding (VENC) set to 130

cm/s and the acquisition plane set parallel to and 1 cm above the pulmonary valve plane. CMR analysis was performed by a single investigator. Quantification of ventricular function was carried out using the Siemens syngo ARGUS Ventricular Function software package with manual drawing of a right ventricular endocardial contour, from which RV end-systolic, end-diastolic, stroke volume and ejection fraction were determined. These values where indexed to body surface area (BSA) using the equation from Kelley et al.[3] The pulmonary regurgitation fraction was calculated using the Siemens syngo ARGUS Flow software package with the rephased images used to draw the analysis ROI and quantification calculated from the phase images. Pulmonary regurgitation fraction was calculated as the ratio of pulmonary retrograde to antegrade flow volume (expressed as a percentage).[4]

Euthanasia and cardiac harvesting

Following a median sternotomy to expose the heart, animals received an intravenous dose of heparin (200 UI/kg, PanPharma) and were euthanised by injection of sodium pentobarbital (10 mL from 200 mg/ml stock). The heart was quickly excised, the aorta cannulated and the myocardium flushed with an ice-cold cardioplegic solution containing (in mM): 110 NaCl, 1.2 $CaCl_2$, 16 KCl, 16 $MgCl_2$, 10 $NaHCO_3$, 9 Glucose supplemented with Heparin (2500 UI/L). The heart and, after careful dissection, the RV wall were weighed. Anterior RV epi- and endocardium samples were snap-frozen into liquid nitrogen for immunohistochemistry and molecular biology studies and kept at -80°C until use.

Optical mapping of cardiac electrical activity

The right coronary artery was canulated at the ostium level and perfused with cardioplegic solution while suturing major arterial leaks. The RV was installed in a chamber, immersed and perfused (20 mL/min) with a modified Krebs-Henseleit solution (37°C) containing (in mM): 130 NaCl, 24 $NaHCO_3$, 1.2 NaH_2PO_4, 1 $MgCl_2$, 5.6 Glucose, 4 KCl, 1.8 $CaCl_2$ constantly gassed with 95% O_2 - 5% CO_2. The preparation was electrically stimulated at 1 Hz in the mid-free wall region using bipolar electrodes at 1.5 time threshold. Contraction was abolished using the electro-mechanical uncoupler blebbistatin

(10 μM, Enzo Life Sciences) before loading with a 10 μM bolus of di-4-ANEPPS (Biotium). The dye was excited using 530 nm LEDs and the voltage-sensitive fluorescent light separated using a 650 ± 50 nm filter. Fluorescent signals were recorded subsequently from the epi- and endocardial surfaces at 1 kHz using a MiCam Ultima CMOS camera (SciMedia USA Ltd) with a spatial resolution of 1 x 1 mm. Pacing frequency was increased from 1 Hz to 5 Hz by 0.5 Hz increments to construct restitution curves (data not shown) and arrhythmias occurring during these protocols were quantified. Prior to data analysis, background fluorescence was substracted and signals were filtered (3 x 3 spatial and 3 x 3 cubic filter). A mask was applied to the camera image in order to remove noisy areas due to remaining epicardial adhesions. Action potential duration was measured at 20% (APD20) and 80% repolarisation (APD80) in 5 x 5 mm regions set on the anterior and posterior side of the RV at mid-height between base and apex. Repolarisation time (RT) dispersion was obtained by subtracting minimum to maximum RT value across the preparation. APD80 dispersion was calculated as the difference between the 95th and the 5th percentile of the APD80 distribution across the RV. Transmural APD20 and APD80 gradient (APD$_{ENDO-EPI}$ gradient) was obtained by subtracting the epicardial APD from the endocardial value of the same region. RV posterior to anterior APD20 and APD80 gradient (APD$_{POST-ANT}$ gradient) was calculated for the epicardium and the endocardium by subtracting anterior APD to the posterior value. Local activation times were calculated at 50% of the action potential upstroke and total epicardial and endocardial activation time was calculated as the time difference between the earliest and the latest activation time across each RV surface. Conduction velocity was measured at proximity of the pacing site by measuring the distance covered by the wavefront over a 20 ms interval in the direction of fast (longitudinal) and slow (transverse) propagation. Arrhythmia dominant frequency was assessed by Fourier transform analysis and regularity index calculated as the transform power at the dominant frequency normalised to total power.

Myocardial collagen content assessment

Immediately after RV dissection, transmural blocks (1.5 x 1.5 cm) of myocardium were taken from the apex of the RV and fixed in 4% paraformaldehyde (Sham, rTOF N=4). The samples were then dehydrated by successive immersions into increasing (70%, 90%, 100%) ethanol concentrations, rinced with Toluene, embedded in paraffin and stored at -20°C until use. After serial transmural sectioning of the sample (8 μm thickness), sections were mounted on slides and stained with Masson's Trichrome using a HMS 70 slide stainer. Images were obtained at a 10X magnification on a Nikon Eclipse 80i microscope equipped with a CCD camera and saved using NIS Elements 3.2 software. Analysis was performed blindly by color thresholding using ImageJ software. Blue-stained areas corresponding to collagen were expressed as a percentage of the section total area. Perivascular and epicardial collagen staining were excluded from the quantification.

Immunohistochemistry

Frozen tissue samples were sectioned (10 μm thickness) and mounted on slides. Following fixation with 4% paraformaldehyde and blocking with 10% normal donkey serum (Jackson ImmunoResearch) in the presence of 0.1% Triton X-100 (Sigma Aldrich), sections were incubated with anti-Connexin-43 antibodies (1:250, Merck-Millipore) overnight at 4°C. After washing with phosphate buffered saline (Sigma Aldrich), sections were incubated with FITC-conjugated donkey anti-mouse antibodies (1:1000, Jackson ImmunoResearch) for 1h at room temperature. Mounting medium (Prolong Gold, ThermoFisher) was added before covering the sections with coverslips. Images were obtained at a 40X magnification on a Nikon Eclipse 80i microscope equipped with a CCD camera and saved using NIS Elements 3.2 software.

Western blot

Tissue samples were homogenised in RIPA buffer (Sigma Aldrich) supplemented with proteases and phosphatases inhibitor cocktails (Sigma Aldrich) and sonicated. Proteins were then extracted by

centrifugation at 12 000 g for 15 min at 4°C, their concentration determined by bicinchoninic acid assay (Thermo Scientific) and kept at -80°C until use. Proteins (50 µg) were separated on 12% acrylamide gels (TGX Stain-Free precast gels, Bio-Rad), under reducing conditions followed by semi-dry transfer (Trans-blot Turbo, Bio-Rad). PVDF membranes were then probed with primary antibodies (Connexin-43, 1:500, Sigma-Aldrich; Kv4.3, 1:200, Merck Millipore) overnight followed by secondary antibodies (Goat anti-rabbit, 1:2000, Bio-Rad). Following total hybridised protein imaging under UV light, Connexin-43 and Kv4.3 specific signals were revealed by enhanced chemiluminescence (Thermo Scientific). Signal quantification was performed using ImageJ (NIH) and specific band intensity was normalised to the total protein intensity of each lane.

RNA extraction

Total RNA was extracted from tissues using QIAzol reagent (Qiagen, USA). RNA was purified and DNase-treated using a Qiagen RNeasy® Kit. RNA purity and integrity, were assessed both by spectrophotometry (NanoDrop ND-1000, NanoDrop Technologies) and nanoelectrophoresis (2100 Bioanalyzer, Agilent Technologies).

Quantitative RT-PCR of ion channels

Sequences for primers were obtained from Ensembl Genome Browser. Primers were designed using Primer designing tool (NCBI) and synthesised at Sigma Aldrich. 1µg of RNA was reversed transcribed using a cDNA Reverse Transcription kit (Life Technologies) according to the manufacturer's protocol. Quantitative PCR was performed in a 25 µL reaction volume (2 µL cDNA, 12,5 µL of SYBR® Premix (BIO-RAD), a volume of 10 µM upstream and downstream primers respectively, and added ddH2O to 25 µL) on the Bio-Rad C 100 Touch Thermal Cycler / CFX96 Real time System. Real-time PCR conditions were as follows: 3 min at 95.0 °C, 40 cycles of denaturation at 95 °C for 30 s followed by 30 s annealing and elongation at 60 °C. Efficiency of primer pairs was previously evaluated. Melting curves were obtained at the end of each run to confirm a single PCR product. All samples were run in

triplicate. Non-template controls were included in each run to exclude contamination and nonspecific amplification. Expression levels of samples were normalised by using a normalisation factor calculated by the software CFX Manager (Bio-Rad). This normalisation factor was calculated based on RT-qPCR results for two selected reference genes, *HPRT1* and *GUSB*.

Microarray profiling of RV endocardium gene expression

cDNA was synthesised from 200 ng of total-RNA using the direct cDNA Labeling System. Aminoallyl-cRNA was synthesised from cDNA using the Superscript Indirect cDNA Labeling System. The cRNA was purified using RNeasy QIAGEN RNeasy® Kit.

Labeling and hybridisation of the cRNA was performed with Agilent Whole Porcine Genome Oligo Microarrays (one-color platform), according to the manufacturer's protocols. The slides were scanned and analysed using the histogram method with default settings in an Agilent G2565C Microarray Scanner System with SureScan Technology. Analysis of microarray data was performed using Genespring®software (Agilent Technologies), with a p-value corrected by Benjamini Hochberg False Discovery Rate (FDR).

Data analysis

Data are expressed as means ± SD. Statistical analysis was performed using SigmaStat software. Statistical differences between groups were tested using One-way ANOVAs followed by Holm-Sidak multiple comparison testing or its non-parametric equivalent and linear regression as appropriate. Statistically significant difference was assumed for P < 0.05.

SUPPLEMENTARY RESULTS

Extracellular matrix remodelling

Our transcriptomic approach revealed a remodelling of the extracellular matrix (ECM) in the anterior RV of rTOF animals (Table S1). ECM constituents such as Keratin 18, cartilage intermediate layer and oligomeric matrix protein were significantly upregulated in rTOF RVs. The expression of tenascin-C, an ECM glycoprotein typically absent in the adult myocardium was found increased in rTOF samples, as seen in endocardial biopsies of patients with dilated cardiomyopathy.[5] Surprisingly, the major cardiac collagen subtypes (type I and III) were not altered in rTOF RVs. Instead we found a significant upregulation of collagen type VIII expression as well as a trend for an upregulation of collagen type XVII (Fold change 2.1, p>0.05) in this region. Moreover, the expression of major metalloproteinase isoforms known to regulate cardiac ECM (e.g. MMP-1, 2, 7, 9) was not altered but we found a decreased expression of metalloproteinase 11. We also found an increased expression of ECM growth factor-related proteins such as fibroblast growth factor 9, inhibin-α, insulin-like growth factor binding protein 2, and transforming growth factor-β regulator 1-like. Potential new markers of ECM remodelling in rTOF RVs were evidenced by our transcriptomic approach, including serpin-family proteins (Nexin-1, Serpine1) known to be critical players in ECM regulation in several organs,[6] or Galectin-1 (LGALS1), a β-galactoside binding lectin from the same family as Galectin-3, a well-described pro-fibrotic protein found to be upregulated in heart failure.[7] In addition, we found an increased expression of Kruppel-like factor 6, a transcription factor recently shown to regulate cardiac fibrosis,[8] and an increase in interleukin 18 expression, a cytokine found to aggravate cardiac fibrosis in a metabolic syndrome rat model.[9]

The regulation of 4 out of 22 genes is expected to favour ECM degradation. The marked increase in the expression (Fold change 9.2) of Frizzled –related protein, an antagonist of the pro-fibrotic Wnt/β-catenin pathway, may represent a feedback mechanism to limit ECM proliferation. Similarly, the

upregulation of Growth hormone releasing hormone (GHRH) expression may contribute to this feedback mechanism as GHRH analogs have been shown to reduce myocardial infarction-related fibrosis.[10] Metallothionein 1A upregulation is also likely to limit fibrosis in rTOF RVs as seen in diabetic mice.[11] Brain Natriuretic peptide (BNP), a heart failure marker synthesised by ventricular myocytes under pressure or volume-overload condition was markedly increased in rTOF RVs (Fold change 13.5) and is known to repress the renin-angiotensin-aldosterone system and thus indirectly exerts anti-fibrotic effects.[12] In addition to BNP, the expression of several proteins known to be regulated by mechanical stress including Tenascin-C,[13] Mitogen-activated protein kinase kinase 1 (MAP2K1)[14] was altered in rTOF pigs, further highlighting the role of RV dilatation in ECM regulation.

Electrophysiological remodelling

Action potential durations measured at early (20%, APD20) and late (80%, APD80) repolarisation stages were regionally altered in rTOF RVs. In the epicardium (Figure S2A-B), rTOF APD20 and APD80 were significantly prolonged in the anterior RV compared to Sham. However, there was a trend for an opposite remodelling in the posterior RV epicardium with shorter APD20 and APD80 in rTOF preparation compared to Sham. This remodelling led to significantly shorter APD80 in the posterior than in the anterior RV of rTOF preparations. This APD remodelling in the rTOF epicardium is likely related to the reduced KCND3/Kv4.3 and increased KCNE2 expression found in this region (see Figure 3) as both would tend to prolong APD. Quantitative RT-PCR revealed no significant change in the other major ion channels involved in the repolarisation phase of the action potential (CACNA1C/Cav1.2, KCNQ1/Kv7.1, KCNH2/Kv11.1, KCNE1/MinK) (Figure S3A).

In the endocardium (Figure S2 C-D), APD20 was significantly shorter in rTOF than in Sham RVs but the APD80 remained unchanged. Our results suggest this endocardial remodelling is related to the increased KCND3/Kv4.3 and KCNE2 expression found in this region (see Figure 3). No significant change was found in the expression of the other ion channels investigated (Figure S3B). Increased

KCND3/Kv4.3 expression is expected to shorten the APD and more specifically at early repolarisation levels while an increase in KCNE2 expression would be expected to prolong the APD at late repolarisation levels. Thus, it is possible to speculate that the increase in KCNE2 expression counteract KCND3/Kv4.3 at late repolarisation stages leading to no significant changes in APD80.

Overall, this APD remodelling led to a significant dispersion of repolarisation on the epicardial surface but also in the transmurality and in the antero-posterior axis of rTOF RV. This specific pattern of APD dispersion is likely to contribute to the increased QT dispersion seen in patients with repaired TOF.[15]

Arrhythmias

Spontaneous arrhythmias, often developing secondary to an increase in pacing frequency during our restitution protocol were more frequently observed in rTOF RVs than in Sham (Figure S4A). Interestingly, there was a negative linear correlation between the number of arrhythmic events and the transverse conduction velocity measured at 1 Hz on the endocardium of rTOF preparations (Figure S4B). Most rTOF arrhythmias (14/16) were sustained VT episodes with the exception of 2 ventricular fibrillation episodes. VT dominant frequency was similar in the anterior and posterior RV regions (Anterior 3.31 ± 1.54 Hz; Posterior 3.89 ± 1.34 Hz) but was lower than in the 2 arrhythmic episodes observed in Sham preparations (Anterior 9.77 ± 1.38 Hz; Posterior 11.12 ± 0.54 Hz). However, VT regularity was heterogeneous across rTOF RVs (Figure S4C), with a lower regularity in the anterior than in the posterior region (Figure S4D).

The lower VT dominant frequency observed in rTOF hearts compared to Sham episodes may be related to the slower, discontinuous activation and heterogeneous repolarisation of the rTOF RV. Despite their lower dominant frequency, rTOF VT episodes displayed a heterogeneous regularity index distribution with less regularity in the anterior RV which appeared to be the most remodelled RV region.

SUPPLEMENTARY TABLES

Gene Symbol	Gene description	Fold Change	Regulation
BNP	Brain natriuretic peptide	13.5	Up
FRZB	Frizzled-related protein	9.2	Up
KRT18	Keratin 18	6.5	Up
CILP	Cartilage intermediate layer protein	4.9	Up
FGF9	Fibroblast growth factor 9	3.9	Up
CTHRC1	Collagen triple helix repeat containing 1	3.6	Up
COL8A1	Collagen type VIII, alpha 1	3.1	Up
TNC	Tenascin-C	2.9	Up
GHRH	Growth hormone releasing hormone	2.8	Up
PN-1	Nexin-1	2.8	Up
MT1A	Metallothionein 1A	2.7	Up
COMP	Cartilage oligomeric matrix protein	2.5	Up
MMP11	Matrix metallopeptidase 11	2.4	Down
INHA	Inhibin, alpha	2.2	Up
LGALS1	Lectin galactoside-binding, soluble	2.2	Up
HYAL1	Hyaluronoglucosaminidase	2.1	Up
IGFBP2	Insulin-like growth factor binding protein 2	2.1	Up
IL18	Interleukin 18	2	Up
SERPINE1	Serpin peptidase inhibitor, clade E, member 1	2	Up
MAP2K1	Mitogen-activated protein kinase kinase 1	1.6	Up
LOC100627866	Transforming growth factor beta regulator 1-like	1.5	Up
KLF6	Kruppel-like factor 6	1.4	Down

Table S1 – Microarray analysis of extracellular matrix-related gene expression in the anterior RV endocardium. Changes in gene expression were determined in rTOF and Sham endocardial samples from the anterior RV using cRNA microarrays. Twenty-two genes constitutive or regulating the extracellular-matrix were differentially expressed (up- or down-regulated) in the rTOF compared to Sham with a fold change between 1.4 and 13.5. Corrected p-values < 0.05 for all 22 genes. Sham N=5, rTOF N=7.

SUPPLEMENTARY FIGURES
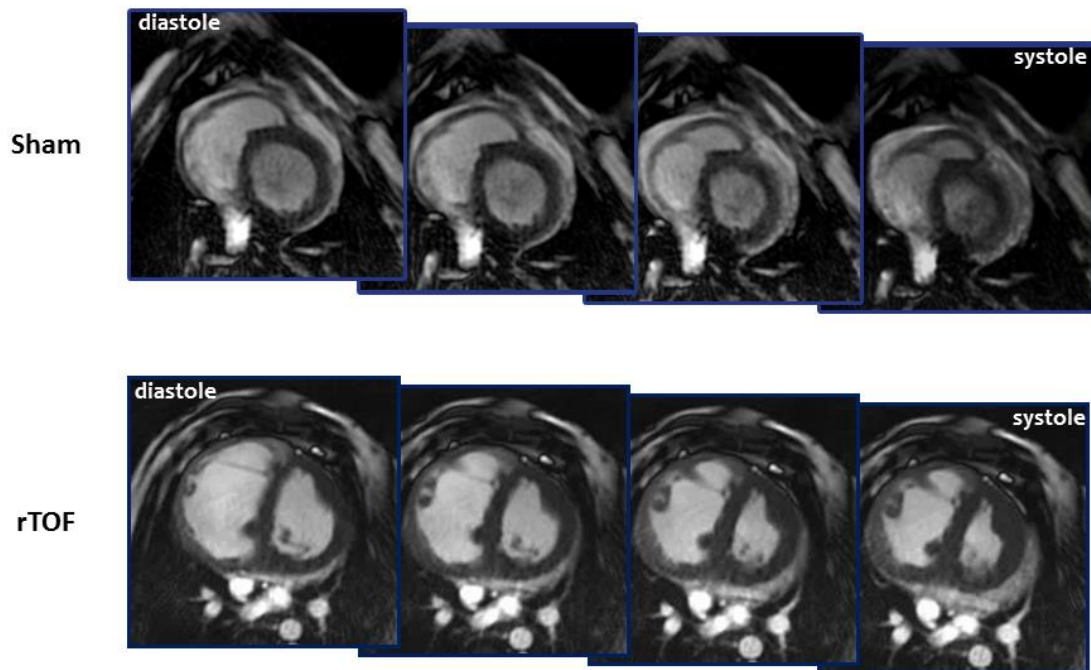
Figure S1 – Sequential images of a Sham and rTOF heart during a cardiac cycle. Cardiac MRI (cMRI) equatorial short axis slices from a cine loop of the heart of a Sham and a rTOF pig showing evenly temporally separated images from diastole (left panel) to systole (right panel). RV hypertrophy and dilatation can be observed in rTOF images. Note the presence of a leftward interventricular septum bulging in rTOF images.
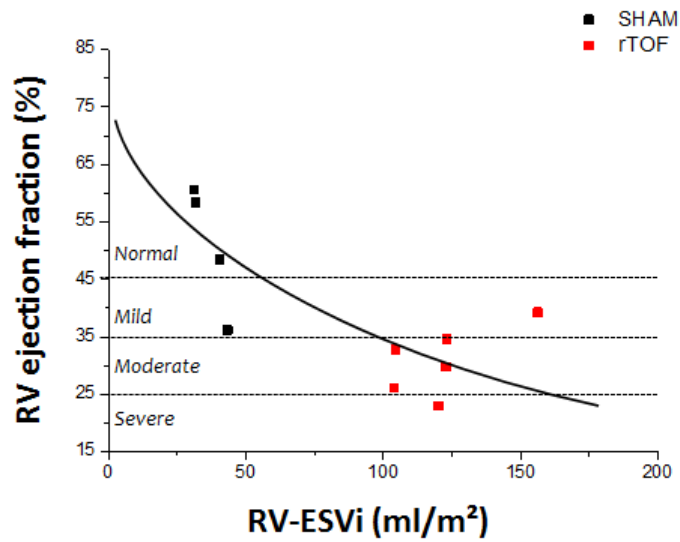
Figure S2 – Right ventricular dysfunction severity grading in rTOF pigs. Relationship between right ventricular end-systolic volume normalised to BSA (RV-ESVi) and RV ejection fraction obtained by MRI. The regression curve and severity grading are those described after cMRI of a population of 100 patients with repaired TOF.[16] According to this grading, rTOF pigs had moderate RV dysfunction. Sham N=4, rTOF N=6.
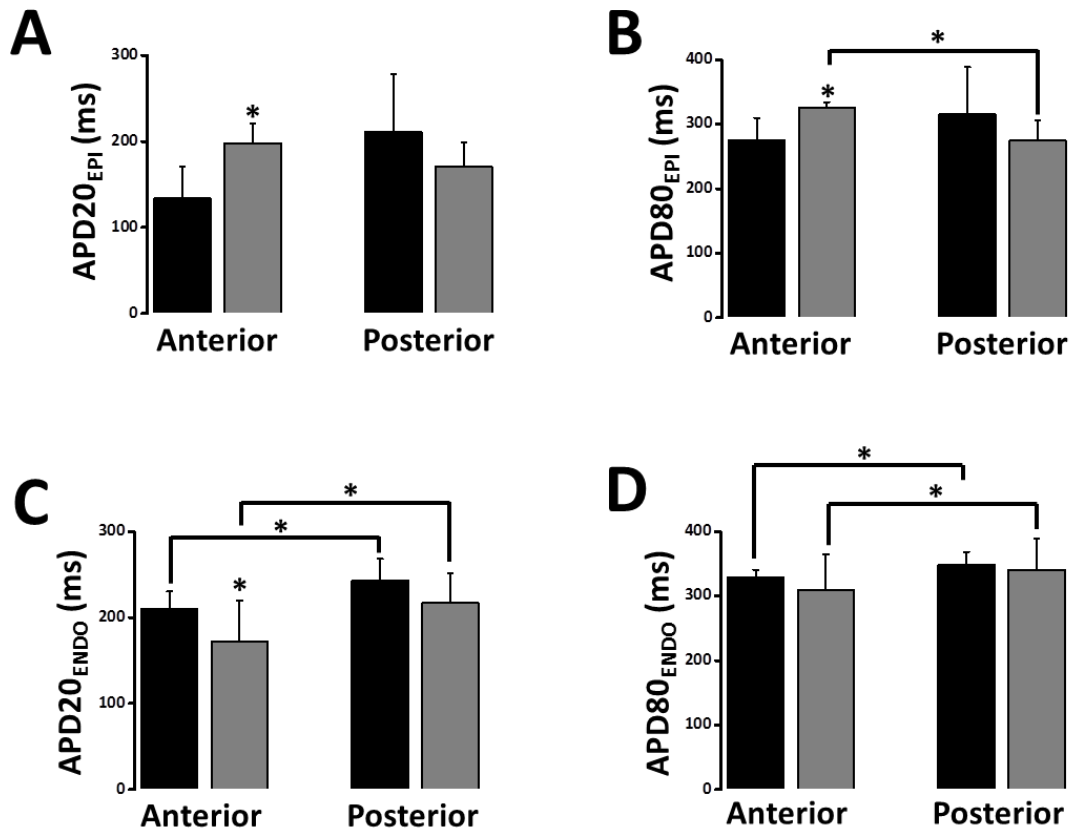
Figure S3 – Regional action potential duration in Sham and rTOF right ventricles. Epicardial APD20 (**A**) and APD80 (**B**) were prolonged in the anterior RV of rTOF (grey) pigs compared to Sham (black). (**C**) Endocardial APD20 was shorter in the anterior rTOF RV than in Sham and posterior rTOF RV. (**D**) APD80 from Sham and rTOF RVs were not different at 1 Hz pacing frequency. Shorter APD80 was observed in the anterior region than in the posterior for both groups. Data are means ± SD. * $P <$ 0.05, Sham N=4, rTOF N=5-6.
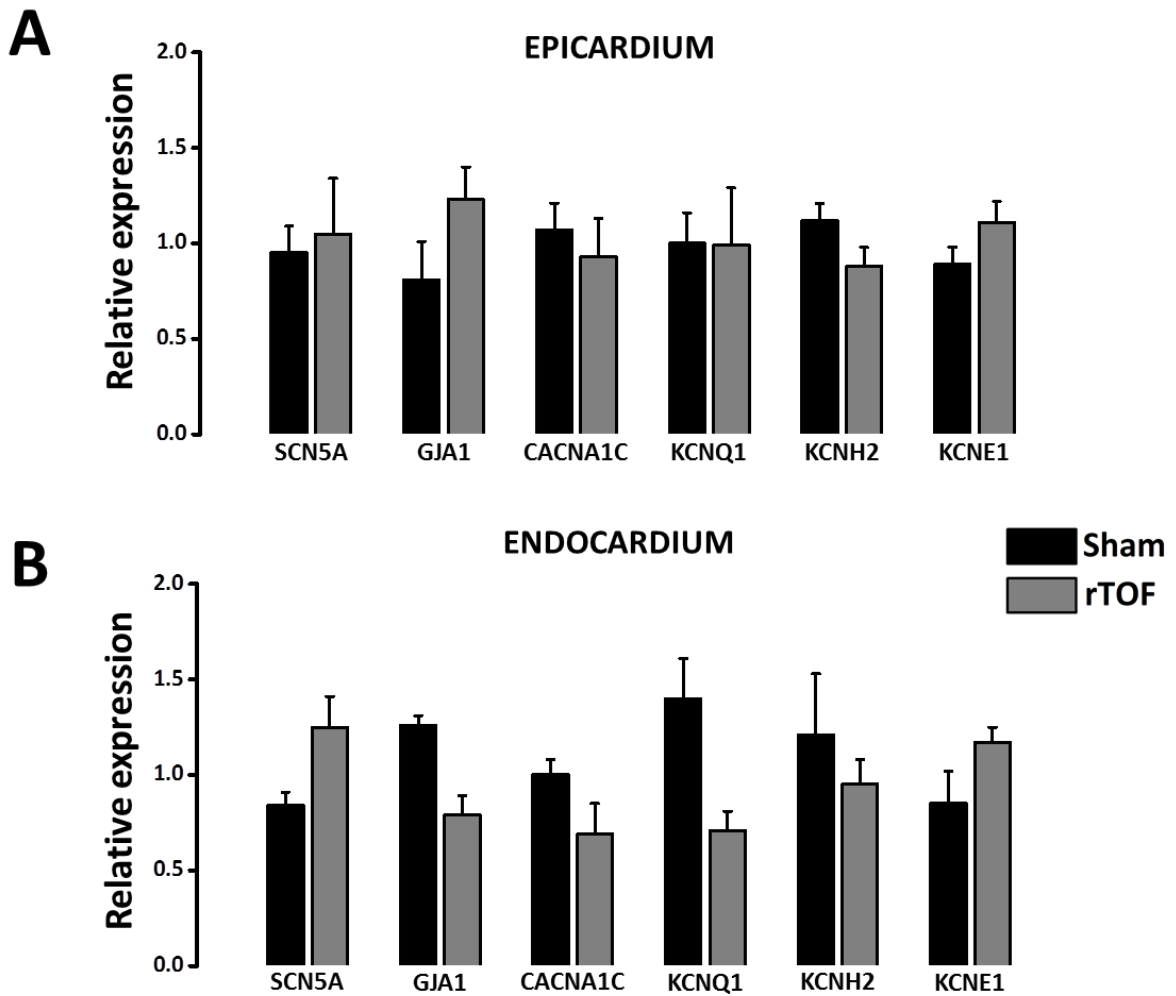
Figure S4 – mRNA expression of ion channels in the anterior RV of Sham and rTOF pigs. mRNA levels for some of the major ventricular ion channels were not significantly altered in the epicardium (**A**) and endocardium (**B**) of rTOF (grey) anterior RV compared to Sham (black). Transcript expression was normalised to the expression of GUSB and HPRT1. Data are means ± SD. Sham N=5, rTOF N=7.
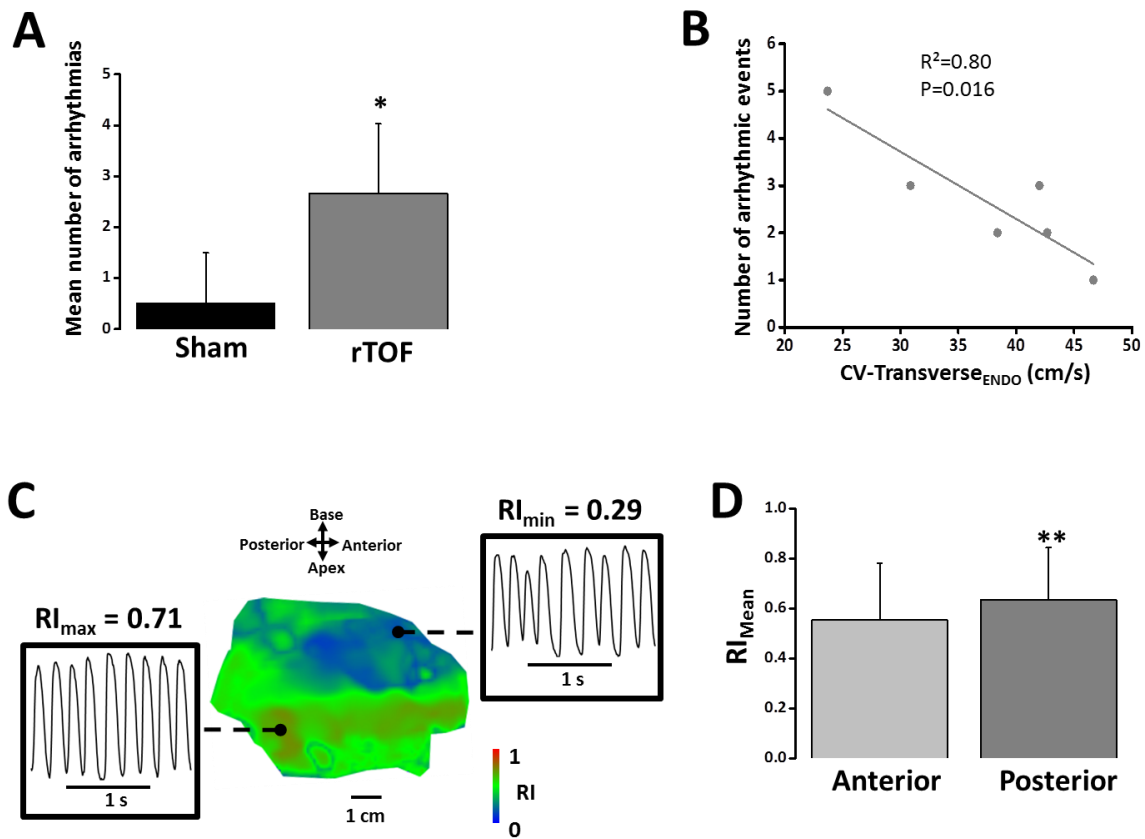
Figure S5 – Quantification and regularity of right ventricular arrhythmias. (**A**) The mean number of spontaneous *ex vivo* arrhythmias was significantly increased in rTOF preparations. (**B**) The total number of arrhythmic events per preparation correlated with endocardial transverse conduction velocity (CV-Transverse$_{ENDO}$) in rTOF RVs. (**C**) Example of a regularity index map from a rTOF RV during a VT episode showing the heterogeneity in arrhythmia regularity across the RV. (**D**) Mean arrhythmia regularity index was lower in RV anterior than in RV posterior region in rTOF preparations (n=14 VT events). Data are means ± SD. **P<0.01, *P<0.05, Sham N=4, rTOF N=6.

SUPPLEMENTAL REFERENCES

1. Thambo JB, Roubertie F, De Guillebon M, et al. Validation of an animal model of right ventricular dysfunction and right bundle branch block to create close physiology to postoperative tetralogy of Fallot. International journal of cardiology 2012;**154**(1):38-42

2. Bogaert J. Cardiac Function. In: Bogaert J, Dymarkowski S, Taylor AM, et al., eds. Clinical Cardiac MRI. Springer ed: Springer, 2012:109-65.

3. Kelley KW, Curtis SE, Marzan GT, et al. Body surface area of female swine. Journal of animal science 1973;**36**(5):927-30

4. Bove T, Bouchez S, De Hert S, et al. Acute and chronic effects of dysfunction of right ventricular outflow tract components on right ventricular performance in a porcine model: implications for primary repair of tetralogy of fallot. Journal of the American College of Cardiology 2012;**60**(1):64-71

5. Tamura A, Kusachi S, Nogami K, et al. Tenascin expression in endomyocardial biopsy specimens in patients with dilated cardiomyopathy: distribution along margin of fibrotic lesions. Heart (British Cardiac Society) 1996;**75**(3):291-4

6. Ghosh AK, Vaughan DE. PAI-1 in tissue fibrosis. Journal of cellular physiology 2012;**227**(2):493-507

7. de Boer RA, Voors AA, Muntendam P, et al. Galectin-3: a novel mediator of heart failure development and progression. European journal of heart failure 2009;**11**(9):811-7

8. Sawaki D, Hou L, Tomida S, et al. Modulation of cardiac fibrosis by Kruppel-like factor 6 through transcriptional control of thrombospondin 4 in cardiomyocytes. Cardiovascular research 2015;**107**(4):420-30

9. Xing SS, Bi XP, Tan HW, et al. Overexpression of interleukin-18 aggravates cardiac fibrosis and diastolic dysfunction in fructose-fed rats. Molecular medicine 2010;**16**(11-12):465-70

10. Kanashiro-Takeuchi RM, Tziomalos K, Takeuchi LM, et al. Cardioprotective effects of growth hormone-releasing hormone agonist after myocardial infarction. Proceedings of the National Academy of Sciences of the United States of America 2010;**107**(6):2604-9

11. Song Y, Wang J, Li Y, et al. Cardiac metallothionein synthesis in streptozotocin-induced diabetic mice, and its protection against diabetes-induced cardiac injury. The American journal of pathology 2005;**167**(1):17-26

12. Levin ER, Gardner DG, Samson WK. Natriuretic peptides. The New England journal of medicine 1998;**339**(5):321-8

13. Yamamoto K, Dang QN, Kennedy SP, et al. Induction of tenascin-C in cardiac myocytes by mechanical deformation. Role of reactive oxygen species. The Journal of biological chemistry 1999;**274**(31):21840-6

14. Lal H, Verma SK, Smith M, et al. Stretch-induced MAP kinase activation in cardiac myocytes: differential regulation through beta1-integrin and focal adhesion kinase. Journal of molecular and cellular cardiology 2007;**43**(2):137-47

15. Gatzoulis MA, Till JA, Redington AN. Depolarization-repolarization inhomogeneity after repair of tetralogy of Fallot. The substrate for malignant ventricular tachycardia? Circulation 1997;**95**(2):401-4

16. Geva T. Repaired tetralogy of Fallot: the roles of cardiovascular magnetic resonance in evaluating pathophysiology and for pulmonary valve replacement decision support. Journal of cardiovascular magnetic resonance : official journal of the Society for Cardiovascular Magnetic Resonance 2011;**13**:9